Electronic Supplementary Information (ESI)

Cerium vanadate hollow spheres mediated polysulfide immobilization and conversion toward lithium-sulfur batteries

Xiang Wu, [a] Jingshuai Xiao, [a] Xuyang Cai, [a] Jiazhuang Chen, [a] Xiao Sun, [a] Tengfei Yang, [a] Yanxia Liu, [b] Xiang Li, [a] Yan Song,* [a] and Chaozheng He* [a]

a Shaanxi Key Laboratory of Optoelectronic Functional Materials and Devices, School of Materials Science and Chemical Engineering, Xi'an Technological University, Xi'an, 710021, China.

b Institute of Science and Technology for New Energy, Xi'an Technological University, Xi'an 710021, China.

*Corresponding authors: E-mail: songyan@xatu.edu.cn, hecz2019@xatu.edu.cn

Experimental

Synthesis of $CeVO_4$ hollow spheres and sulfur cathodes

$Ce(NO_3)_3 \cdot 6H_2O$ (1 mmol) was dissolved in deionized water under magnetic stirring until a clear solution was formed. Subsequently, 500 mg polyvinyl pyrrolidone (PVP) and 1.5 g urea were added sequentially, with each component stirred at room temperature for 30 minutes. The resulting solution was transferred to a 50 mL Teflon-lined autoclave and maintained at 120 °C for 3 h. After cooling to room temperature, the products were collected and washed with deionized water and ethanol, after cooling to room temperature, the products were collected, washed with deionized water and ethanol, and then redispersed in deionized water for further use.

1.0 mmol of NH_4VO_3 was added to the above solution and transferred to a 50 mL Teflon-lined autoclave. The mixture maintained at 180 °C for 12 h, followed by natural cooling to room temperature. the products were collected and washed with deionized water and absolute ethanol, and finally dried at 80 °C overnight.

The $CeVO_4$-S composite was synthesized via a melt-diffusion method. Briefly, $CeVO_4$ and sulfur powders were thoroughly ground at a weight ratio of 1:4 and then heated at 155 °C for 12 h.

Synthesis of Li_2S_6 solution

The Li_2S_6 solution was obtained by dissolving elemental sulfur and Li_2S at a molar ratio of 5:1 in a mixed solvent of 1,2-dimethoxyethane (DME) and 1,3-dioxolane (DOL) (v/v = 1:1), followed by continuous stirring at 60 °C for 12 h.

Materials characterization

The crystal structure was characterized by X-ray diffraction system (XRD, Bruker D8). Meanwhile, the surface chemical composition of was characterized by X-ray photoelectron spectroscopy (XPS, an ESCALAB 250Xi spectrometer). The surface

morphology of the electrode was characterized by scanning electron microscope (SEM, JSM-7610F). The microstructure of the electrode was characterized by Transmission electron microscope (TEM, JEM-2100). The specific surface areas and pore volumes of all samples were measured by the Brunauer-Emmett-Teller (BET) method using nitrogen adsorption and desorption isotherms on a Micromeritics (JW-BK122-B, JWGB SCI. & Tech).

Battery assembly and electrochemical measurements

The cathode was fabricated by mixing $CeVO_4$-S (with a sulfur content of 80 wt%), conductive carbon (Super P), and polyvinylidene fluoride (PVDF) at a mass ratio of 7:2:1 in 1-methyl-2-pyrrolidinone (NMP) to form a homogeneous slurry. The slurry was uniformly coated onto aluminum foil and punched into disks with a diameter of 12 mm to obtain sulfur cathodes. The electrodes were then dried under vacuum at 60 °C overnight. The active sulfur loading was about 2 mg cm^{-2}. A high-sulfur-loading cathode with a sulfur loading of 4.7 mg cm^{-2} was fabricated by regulating the coating thickness. As a comparison, pure S cathode were prepared as described above in the same way (omitting the step of adding catalyst).

The 2032 type coin cells were assembled in an Ar-filled glove box, using active sulfur as the cathode, lithium metal foil as the anode, and Celgard 2400 as the separator. The electrolyte consists of a solution of 1,3-dioxolane (DOL) and dimethyl ether (1:1 by volume) containing 1 M lithium dilithium (trifluoromethane sulfonyl) imide (LiTFSI) and 1wt% $LiNO_3$. The electrolyte intake is approximately 40 μL in per coin battery. Galvanostatic charge–discharge tests were carried out using a Neware battery testing system within a voltage range of 1.7-2.8 V. Cyclic voltammetry (CV) and electrochemical impedance spectroscopy (EIS) measurements were performed using a CHI660E electrochemical workstation. The EIS tests were conducted over a frequency

range of 100 kHz to 0.01 Hz with an amplitude of 5 mV. During the GITT measurement, the cell was discharged at a rate of 0.1 C for 15 minutes, followed by a 1 h relaxation period. This procedure was repeated until the voltage dropped below 1.7 V, indicating the completion of the discharge process. During charging, the cell was charged at a rate of 0.1 C for 15 minutes, followed by a 1 h relaxation period, and the cycle was continued until the voltage exceeded 2.8 V.

Supplementary Figures

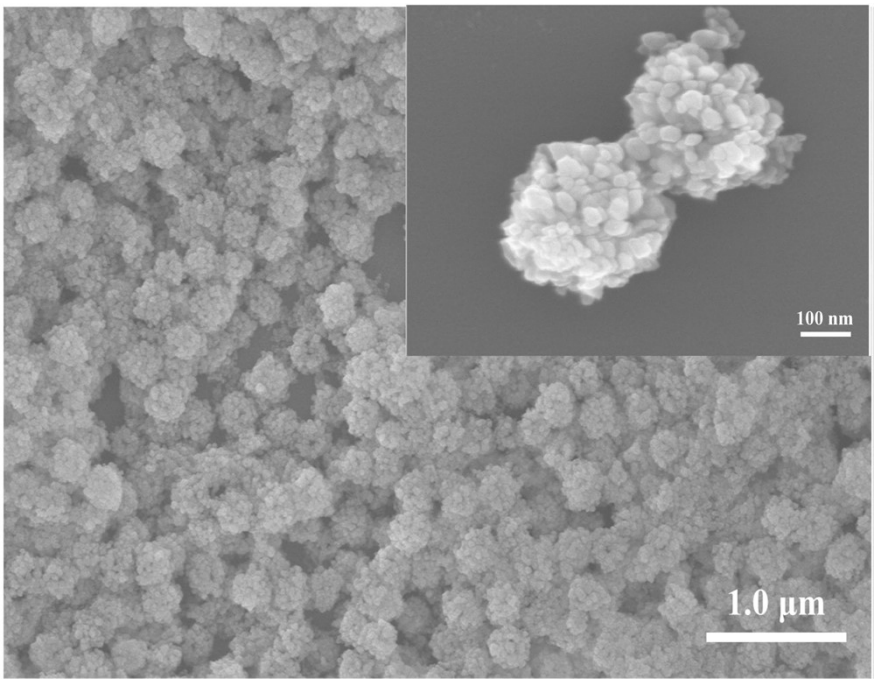

Fig. S1 SEM images of $CeVO_4$.

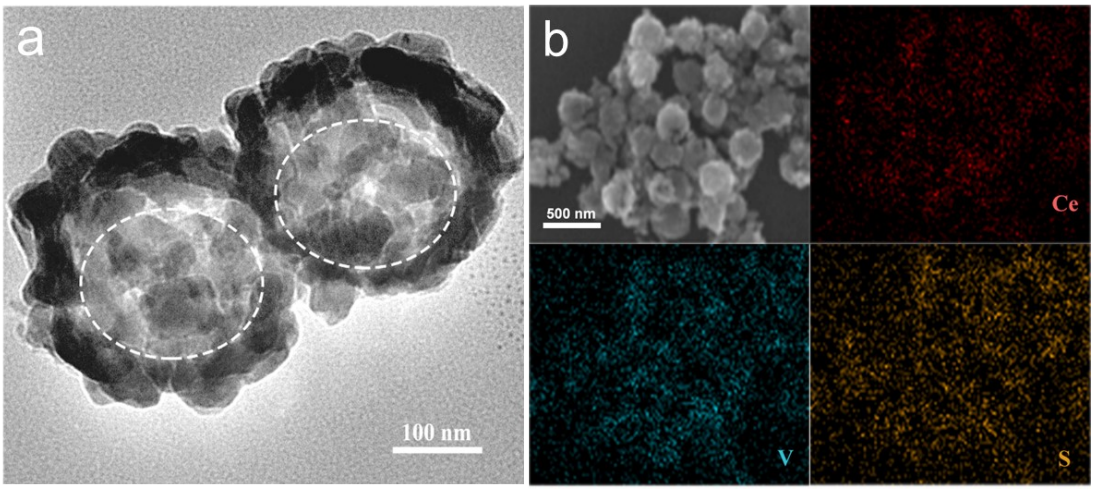

Fig. S2 (a) TEM and (b) EDS elemental mapping images of the $CeVO_4$-S.

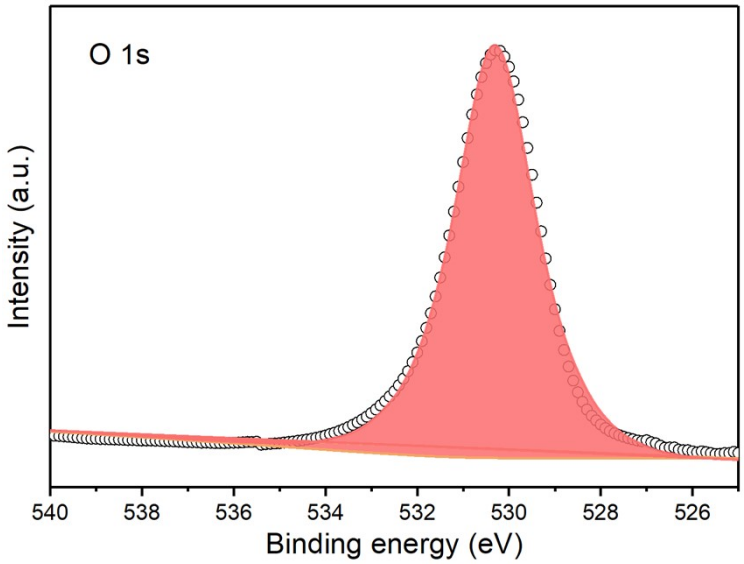

Fig. S3 O 1s high-resolution XPS spectrum of $CeVO_4$.

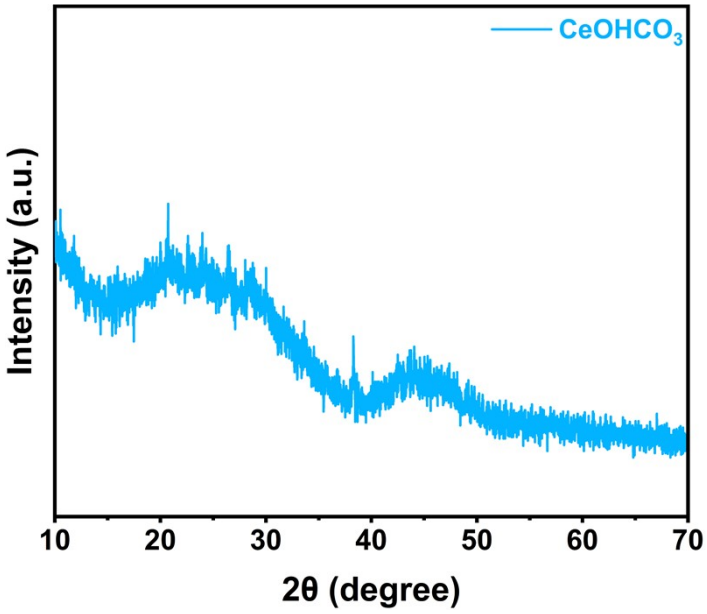

Fig. S4 XRD pattern of the $CeOHCO_3$.

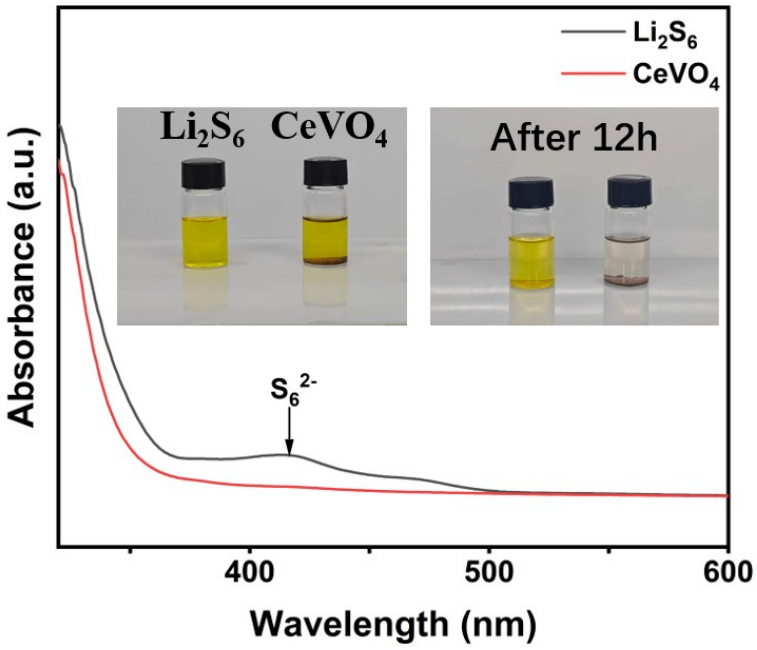

Fig. S5 UV-vis spectra of Li_2S_6 solution before and after adsorbed by $CeVO_4$. Inset: digital photographs of Li_2S_6 adsorption test.

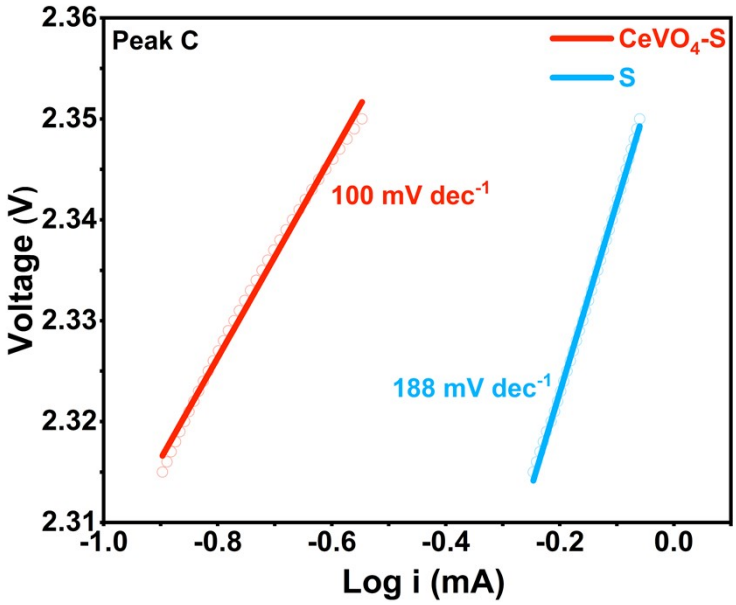

Fig. S6 Corresponding Tafel plots from the CV curves.

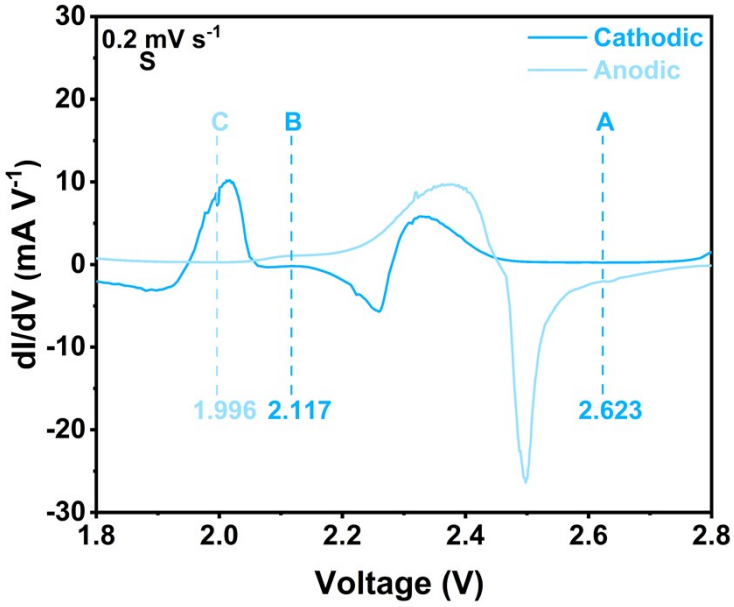

Fig. S7 Differential CV curves of batteries assembled with S cathodes

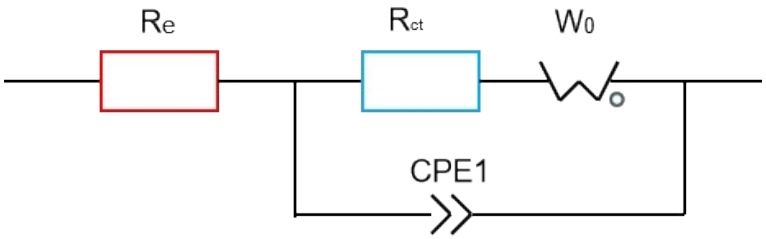

Fig. S8 The well-fitted Randles EIS equivalent circuits.

Note: The meaning of each component in the diagram is shown below: R_e: The internal resistance of the electrolyte; R_{ct}: The charge-transfer resistance, related to the electrode reaction kinetics; CPE1: Capacitance of the electrode bulk in high-frequency region; W_o: The semi-infinite Warburg diffusion impedance.

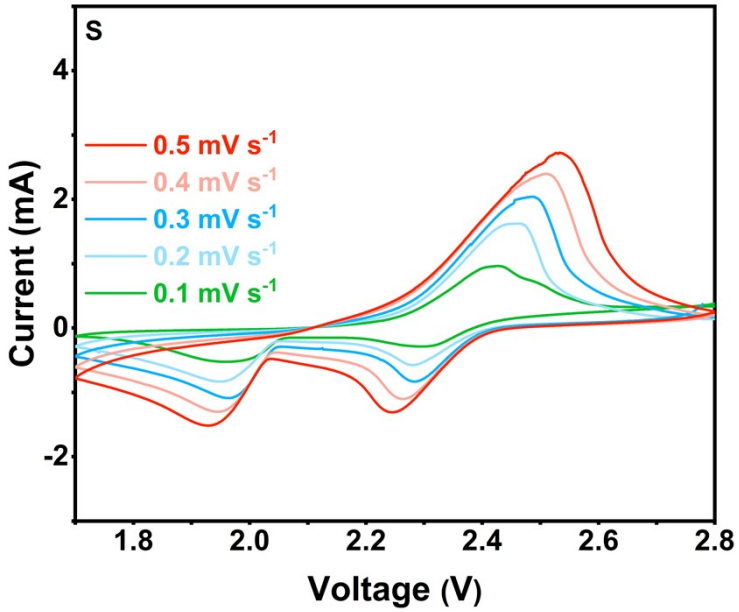

Fig. S9 Cyclic voltammetry curves of batteries assembled with S cathodes.

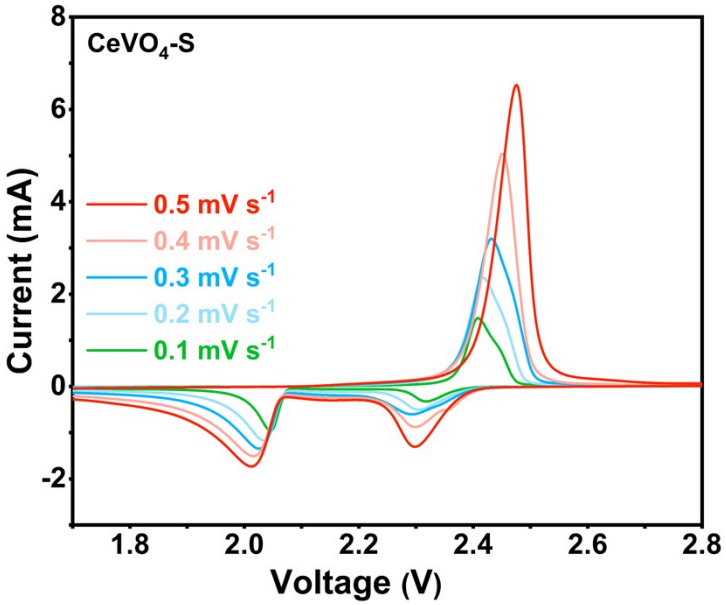

Fig. S10 Cyclic voltammetry curves of batteries assembled with $CeVO_4$-S cathodes.

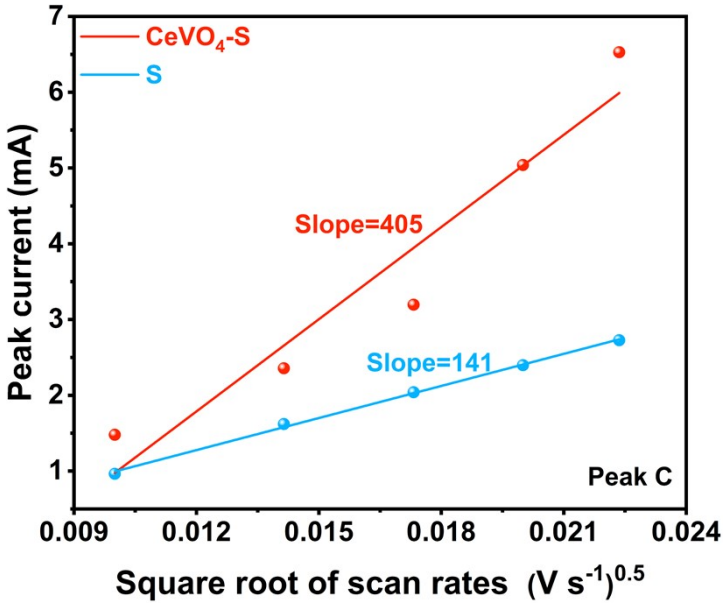

Fig. S11 The peak C current versus the square root of scan rates.

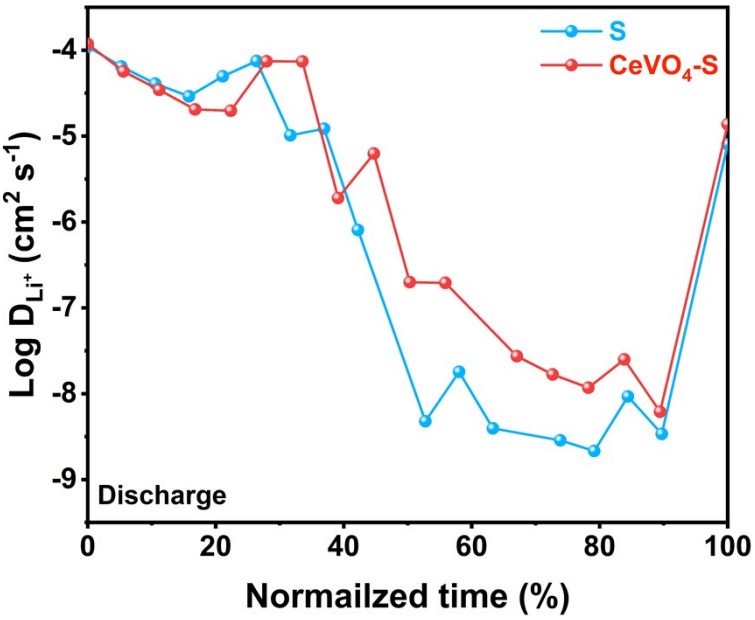

Fig. S12 Li^+ transport coefficient during the discharge process

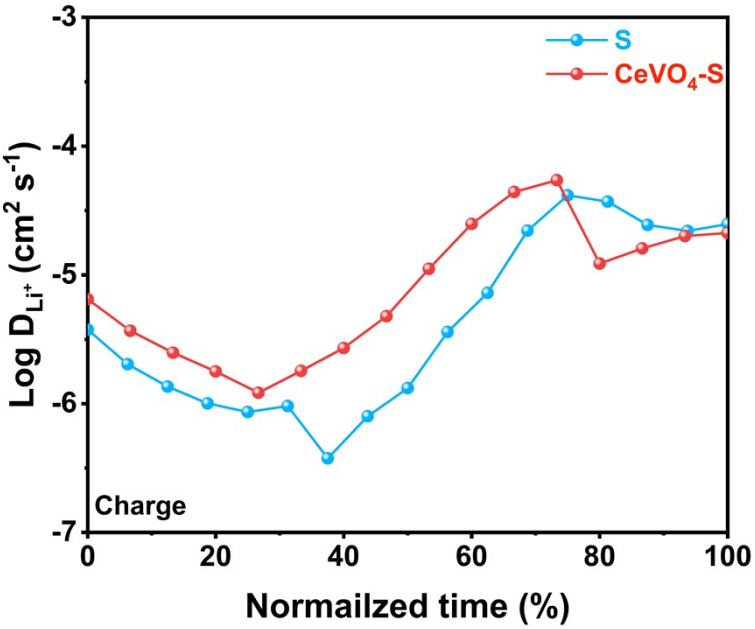

Fig. S13 Li^+ transport coefficient during the charge process

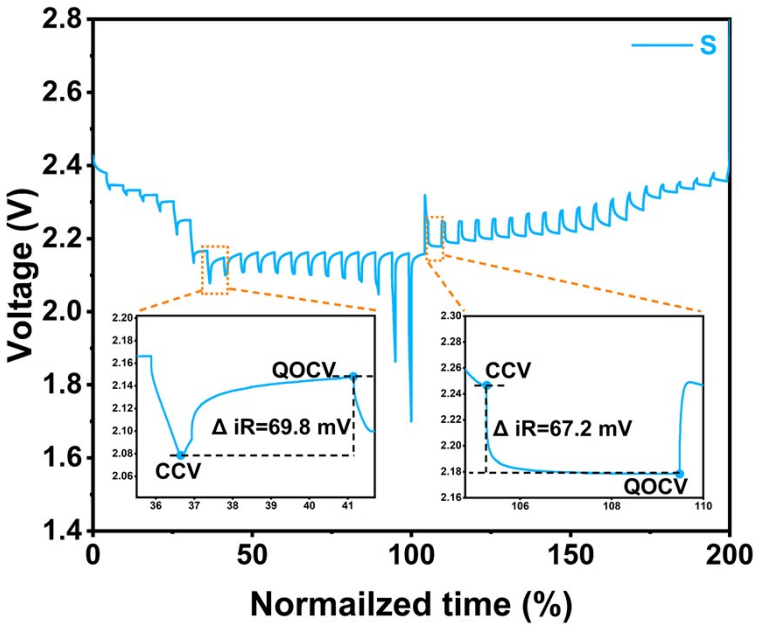

Fig. S14 GITT profiles of the S cathode during the charge and discharge processes

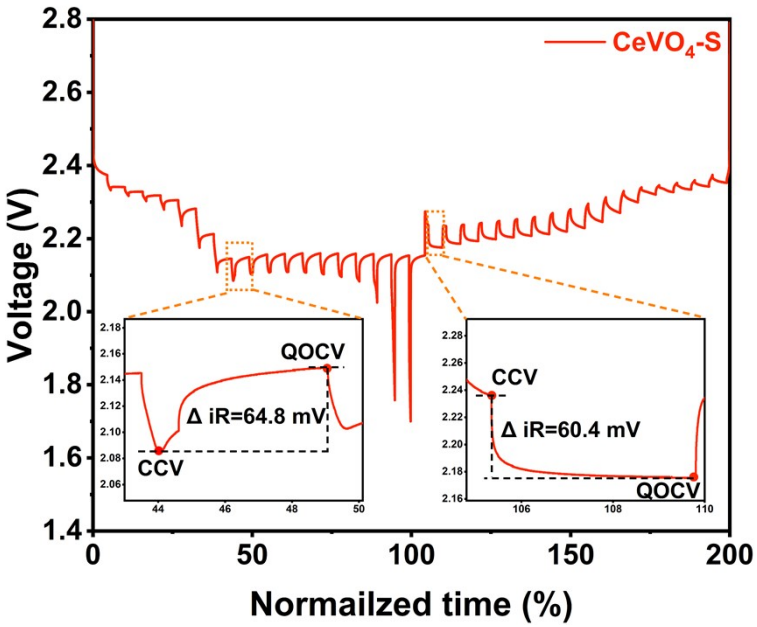

Fig. S15 GITT profiles of the $CeVO_4$-S cathode during the charge and discharge processes

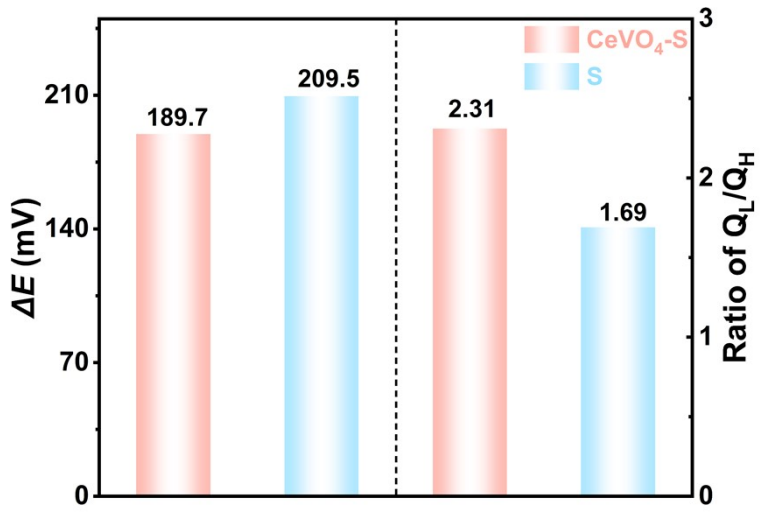

Fig. S16 Comparison of the corresponding *ΔE* and Q_L/Q_H at 0.2 C.

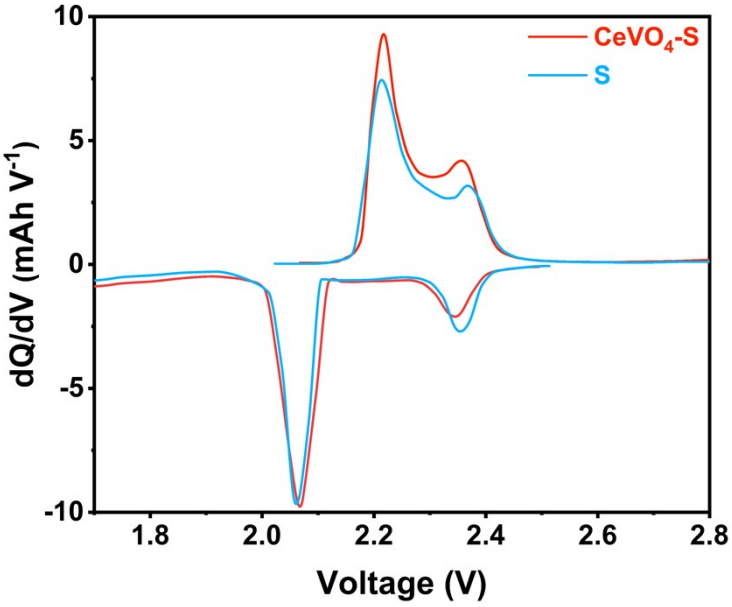

Fig. S17 Differential capacity (dQ/dV) curves at 0.2 C.

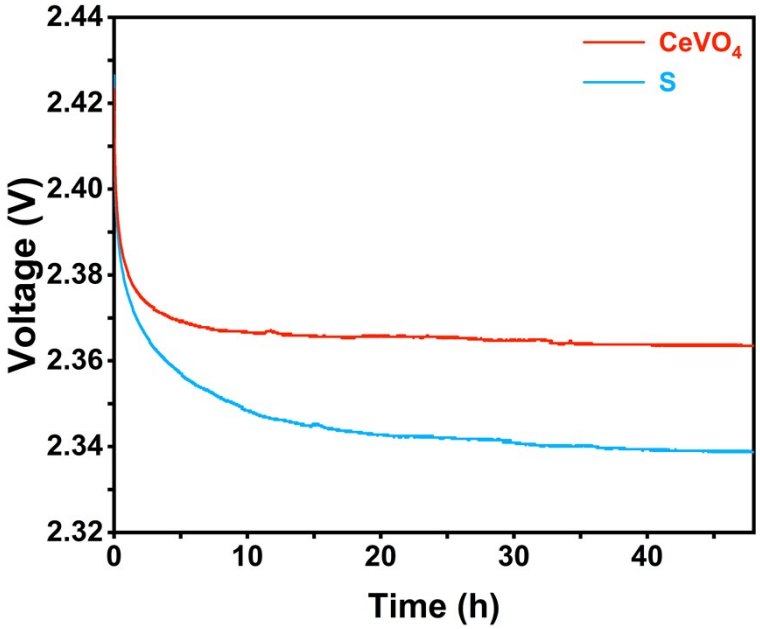

Fig. S18 Open-circuit voltage profiles after resting for 2 days following 5 cycles.

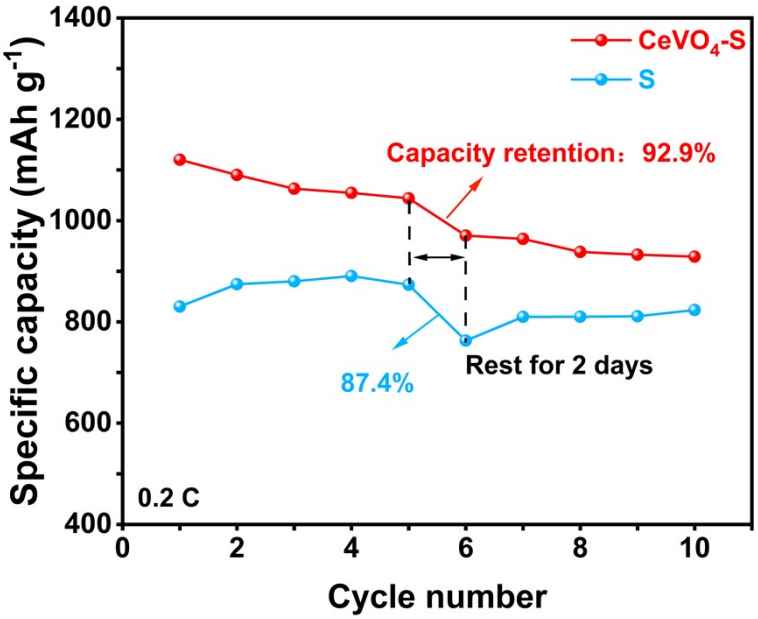

Fig. S19 Self-discharge performance of the Li-S batteries with $CeVO_4$-S and S cathodes.

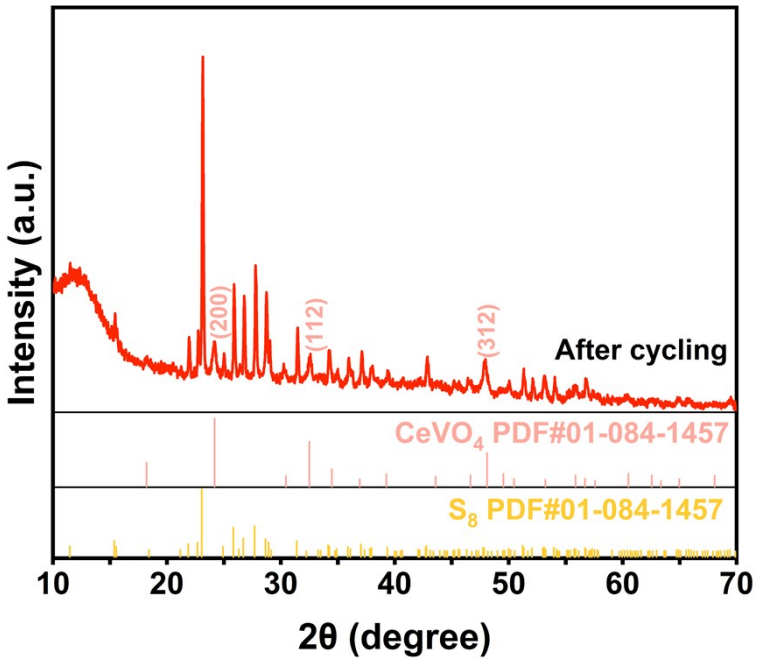

Fig. S20 XRD pattern of the $CeVO_4$-S cathode after cycles.

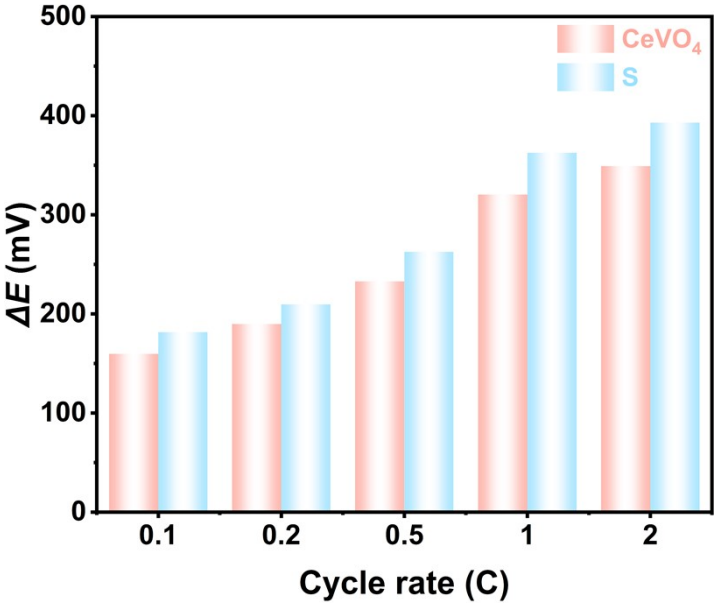

Fig. S21 Comparing the corresponding *ΔE* at 0.1-2 C.

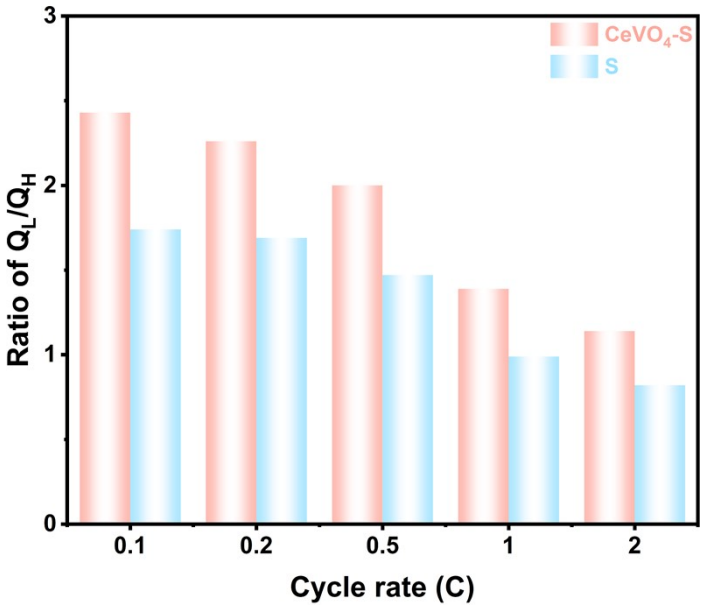

Fig. S22 Comparing the corresponding Q_L/Q_H at 0.1-2 C.

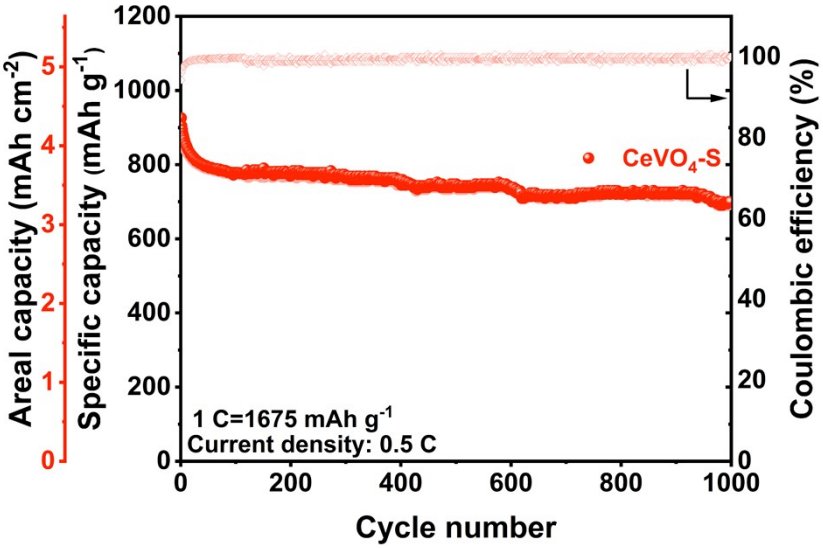

Fig. S23 Cycles performance of the $CeVO_4$-S cathode over 1000 cycles at 0.5 C with a sulfur loading of 4.7 mg cm^{-2}.

Table S1 Comparison of Performance of Advanced Li-S Battery Catalysts.

Materials	Sulfur loading (mg cm^{-2})	Initial capacity (mAh g^{-1})	Rate (C)	Cycle number	Decay rate	Ref.
$CeVO_4$-S	2.0	1114	0.2	900	0.027%	This work
YHS@C	2.1	912.5	0.5	200	0.038%	[1]
S/rGO-$La(OH)_3$	2.8	1160	0.2	100	0.222%	[2]
Sm_2O_3/CA	2.2	1322	0.2	300	0.115%	[3]
MWCNTs/CeO_2	1.8-2.0	898	0.2	300	0.140%	[4]
CeF_3-20/CF	1.6	1015	0.2	100	0.064%	[5]
GB-Y	0.6	1201.5	0.2	100	0.297%	[6]
NCFI@T_{150}	1.5	1127	0.2	200	0.090%	[7]

References

1. P. Zeng, M. Chen, J. Luo, H. Liu, Y. Li, J. Peng, J. Li, H. Yu, Z. Luo, H. Shu, C. Miao, G. Chen and X. Wang, *ACS Appl. Mater. Interfaces*, 2019, **11**, 42104–42113.
2. Y. Tian, Y. Zhao, Y. Zhang, L. Ricardez-Sandoval, X. Wang and J. Li, *ACS Appl. Mater. Interfaces*, 2019, **11**, 23271–23279.
3. H. Sheng, X. Li, B. Huang, J. Wang, X. Li and Y. Hua, *ChemPlusChem*, 2019, **84**, 838–844.
4. W. Zhu, Z. Zhang, J. Wei, Y. Jing, W. Guo, Z. Xie, D. Qu, D. Liu, H. Tang and J. Li, *J. Membr. Sci.*, 2020, **597**, 117646.
5. K. Zou, N. Li, X. Dai, W. Jing, M. Shi, C. Lu, Q. Tan, Y. Xin, J. Sun, Y. Chen and Y. Liu, *ACS Appl. Nano Mater.*, 2020, **3**, 5732–5742.
6. F. Zhou, Y. Mei, Q. Wu, H. Li, J. Xu and H. Chen, *Energy Storage Mater.*, 2024, **67**, 103315.
7. S. Yang, D. Jiang, Q. Su, S. Yuan, Y. Guo, K. Duan, M. Xiang, J. Guo, W. Bai and S. Chou, *Adv. Energy Mater.*, 2024, **14**, 2400648.